Spatially-Resolved Dynamics of the Amplitude Schmid-Higgs Mode in Disordered Superconductors

P. A. Nosov,[1] E. S. Andriyakhina,[2] and I. S. Burmistrov[3,4]
[1]Department of Physics, Harvard University, Cambridge, Massachusetts 02138, USA
[2]Freie Universität Berlin, Dahlem Center for Complex Quantum Systems and Fachbereich Physik, Arnimallee 14, Berlin, 14195, Germany
[3]L.D. Landau Institute for Theoretical Physics, Akademika Semenova av.1-a, Chernogolovka, 142432, Russia
[4]Laboratory for Condensed Matter Physics, HSE University, Moscow, 101000, Russia

(Received 24 September 2024; revised 10 March 2025; accepted 14 July 2025; published 30 July 2025)

We investigate the spatially-resolved dynamics of the collective amplitude Schmid-Higgs (SH) mode in disordered s-wave superconductors and fermionic superfluids. By analyzing the analytic structure of the zero-temperature SH susceptibility in the complex frequency plane, we find that, when the coherence length greatly exceeds the mean free path, (i) the SH response at fixed wave vectors exhibits late-time oscillations decaying as $1/t^2$ with frequency 2Δ, where Δ is the superconducting gap; (ii) subdiffusive oscillations with a dynamical exponent $z = 4$ emerge at late times and large distances; and (iii) spatial oscillations at a fixed frequency decay exponentially, with a period that diverges as the frequency approaches 2Δ from above. When the coherence length is comparable to the mean free path, additional exponentially-decaying oscillations at fixed wave vectors appear with a frequency above 2Δ. Furthermore, we show that the SH mode induces an extra peak in the third-harmonic generation current at finite wave vectors. The frequency of this peak is shifted from the conventional resonance at Δ, thereby providing an unambiguous signature of order parameter amplitude dynamics.

DOI: 10.1103/x12p-q7bj

Investigating the collective excitations in superconductors provides crucial insights into the complex structure of their order parameter and associated dynamical responses [1–6]. Unlike the well-studied phase fluctuations, the collective dynamics of the order parameter amplitude [so-called Schmid-Higgs (SH) mode] has received much less attention due to experimental challenges in its detection, primarily caused by its decoupling from density fluctuations. However, recent advances in terahertz and Raman spectroscopic probes have made direct observation of the SH mode more accessible [7–11], in turn prompting a renewed wave of theoretical interest in the amplitude fluctuations [12–30].

The properties of the SH mode in a disorder-free limit are relatively well established in both three-dimensional (3D) [17,24,31,32] and two-dimensional (2D) [17,18,29] systems, across weak and strong coupling regimes. However, real materials inevitably contain impurities or other structural imperfections, making it imperative to understand how disorder influences the fluctuations of the superconducting order parameter. Despite extensive research of collective responses in dirty superconductors [26,33–43], a comprehensive description of the spatially-resolved SH dynamics in this limit is still lacking. In particular, the dispersion relation and the associated long-distance and late-time oscillatory behavior of the SH mode in the presence of disorder remain unknown. Another open question is how the SH mode contributes to the nonlinear current response at finite wave vectors.

The goal of the present Letter is to fill this gap by examining the nonanalyticities of the $T = 0$ disorder-averaged SH susceptibility $\chi_{\mathrm{SH}}(z, \boldsymbol{q})$ as a function of complex frequency and momentum. This susceptibility quantifies the dynamical response of the order parameter amplitude $|\Delta(t, \boldsymbol{r})|$ that arises when external perturbations disturb it from its equilibrium state. Our approach is based on the BCS model with impurities, assuming a local attractive coupling λ that induces an s-wave, spin-singlet superconducting state with a zero-temperature gap Δ. For concreteness, we consider the following Hamiltonian density

$$\mathcal{H} = \sum_{\sigma} \psi_{\sigma}^{\dagger} \left(-\frac{(\nabla - i\boldsymbol{A})^2}{2m} - \mu + V(\boldsymbol{r}) \right) \psi_{\sigma} - \frac{\lambda}{\nu} \psi_{\uparrow}^{\dagger} \psi_{\downarrow}^{\dagger} \psi_{\downarrow} \psi_{\uparrow}. \tag{1}$$

Here, $\sigma = \uparrow/\downarrow$ labels spin degrees of freedom, ν is the density of states at the Fermi level in the normal state, $\lambda > 0$ is the dimensionless BCS coupling constant, $\psi_{\sigma}(\boldsymbol{r})$ is the electron field, $\boldsymbol{A}$ is the vector potential, and $V(\boldsymbol{r})$ is a white-noise Gaussian random potential that induces elastic scattering rate $1/\tau$. We assume that both $1/\tau$ and the superconducting gap Δ are much smaller than the Fermi

energy, $\mu = mv_F^2/2$ (v_F is the Fermi velocity and m is the electron mass), which allows us to linearize the electron dispersion and treat impurity scattering within the self-consistent Born approximation. The ratio $\Delta\tau$ is used to interpolate between the dirty ($\Delta\tau \ll 1$) and clean ($\Delta\tau \gg 1$) regimes. Under these conditions, the interplay of superconductivity and disorder is treated at the level of Anderson's theorem [44–46], disregarding more subtle effects such as interference-induced corrections [47–50] or spatial inhomogeneity of the order parameter and Lifshitz tails below the spectral edge [51–53].

SH susceptibility—The collective dynamics of the superconducting order parameter is described by the standard Ginzburg-Landau functional obtained from Eq. (1) at $\boldsymbol{A} = 0$, with its quadratic part encoding Gaussian fluctuations of the amplitude $|\Delta|$ around its mean-field value [54]:

$$S_{\Delta\Delta} = \int_r \sum_n \Delta(i\omega_n, \boldsymbol{r}) \chi^{-1}_{\mathsf{SH}}(i\omega_n, \boldsymbol{r}, \boldsymbol{r}') \Delta(-i\omega_n, \boldsymbol{r}')$$
$$\chi^{-1}_{\mathsf{SH}}(i\omega_n, \boldsymbol{r}, \boldsymbol{r}') = \lambda^{-1}\delta(\boldsymbol{r}-\boldsymbol{r}') - \Pi_{\Delta\Delta}(i\omega_n, \boldsymbol{r}, \boldsymbol{r}'), \tag{2}$$

where $\omega_n = 2\pi T n$ is the bosonic Matsubara frequency, χ_{SH} is the real space Matsubara SH susceptibility in a given disorder realization, and $\Pi_{\Delta\Delta}(i\omega_n, \boldsymbol{r}, \boldsymbol{r}')$ is the Fourier transform of the imaginary time correlation function $(\pi\nu)^{-1}\langle \mathcal{T}\hat{\Delta}(\tau, \boldsymbol{r})\hat{\Delta}(0, \boldsymbol{r}')\rangle$. Here $\hat{\Delta}(\tau, \boldsymbol{r})$ is the s-wave, spin-singlet order parameter amplitude.

The expectation value is taken in the standard BCS state with the uniform mean-field order parameter Δ determined via the gap equation $1 = \pi\lambda T \sum_m 1/E_{\varepsilon_m}$. Here $E_{\varepsilon_m} = \sqrt{\varepsilon_m^2 + \Delta^2}$, and $\varepsilon_m = 2\pi T(m + 1/2)$ is the fermionic Matsubara frequency.

In this setup, the disorder-averaged Matsubara SH susceptibility $\chi_{\mathsf{SH}}(i\omega_n, \boldsymbol{q})$ is given by [56]

$$\frac{1}{\chi_{\mathsf{SH}}} = \pi T \sum_m \left\{ \frac{1}{E_{\varepsilon_m}} - S_{\boldsymbol{q}}(E_{\varepsilon_m} + E_{\tilde{\varepsilon}_m}) \left[1 + \frac{\varepsilon_m \tilde{\varepsilon}_m - \Delta^2}{E_{\varepsilon_m} E_{\tilde{\varepsilon}_m}} \right] \right\}, \tag{3}$$

where $\tilde{\varepsilon}_m = \varepsilon_m + |\omega_n|$. This expression assumes $q \ll mv_F$, but fully captures the crossover between the diffusive and ballistic scales through the structure factor $S_{\boldsymbol{q}}(E)$. It is given by $S^{\mathrm{2D}}_{\boldsymbol{q}}(E) = 1/(|\mathcal{E}| - 1/\tau)$ for a 2D system and by $S^{\mathrm{3D}}_{\boldsymbol{q}}(E) = 1/(v_F q/\arg\mathcal{E} - 1/\tau)$ in 3D, where $\mathcal{E} = E + 1/\tau + iv_F q$. In the diffusive limit, $v_F q,\ E \ll 1/\tau$, the structure factor in Eq. (3) reduces to [4,33,55]

$$S_{\boldsymbol{q}}(E) = 1/(Dq^2 + E), \qquad D = v_F^2\tau/d, \tag{4}$$

where $d = 2,\ 3$ is the dimensionality. At $q = 0$, Eq. (3) reduces to its clean limit for any $\Delta\tau$ as a manifestation of Anderson's theorem.

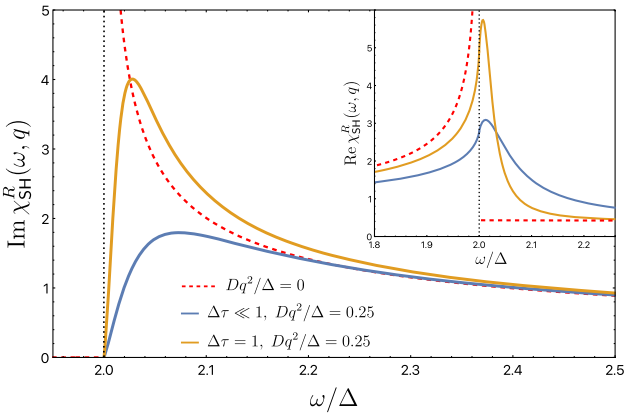

FIG. 1. Spectral function $\mathrm{Im}\chi^R_{\mathsf{SH}}(\omega, \boldsymbol{q})$ for $Dq^2/\Delta = 0.25(\xi q = 0.5)$. The blue (orange) curve corresponds to $\Delta\tau \ll 1(\Delta\tau = 1)$ in 2D. The dotted line indicates the continuum edge. The dashed red line corresponds to $q = 0$ independent of $\Delta\tau$. Inset: $\mathrm{Re}\chi^R_{\mathsf{SH}}(\omega, \boldsymbol{q})$ for the same parameters.

The retarded SH susceptibility $\chi^R_{\mathsf{SH}}(\omega, \boldsymbol{q})$ at $T = 0$ is obtained from Eq. (3) in a standard way [56]. The branch cuts are chosen along the real axis such that for any real $|E| \geq \Delta$ we have $\sqrt{\Delta^2 - (E \pm i0)^2} = \mp i\mathrm{sgn}(E)\sqrt{E^2 - \Delta^2}$. If extended to the lower half-plane as well, the above choice of the branch cut defines the *physical* Riemann sheet of $\chi_{\mathsf{SH}}(z, \boldsymbol{q})$, with its imaginary part changing discontinuously across the cut along the real axis at $|\mathrm{Re}z| \geq 2\Delta$ and vanishing for $\mathrm{Im}\,z = 0, |\mathrm{Re}z| \leq 2\Delta$ due to the presence of the superconducting gap (see Fig. 1). The resulting Cauchy representation of $[\chi_{\mathsf{SH}}(z, \boldsymbol{q})]^{-1}$ on the physical sheet is given by

$$\frac{1}{\chi_{\mathsf{SH}}} = \int_{-\infty}^{+\infty} \frac{d\varepsilon}{\pi} \left[\frac{\rho_{\boldsymbol{q}}(|\varepsilon|)\mathrm{sgn}\varepsilon}{\varepsilon - z} + \frac{\pi/2}{\sqrt{\varepsilon^2 - 4\Delta^2}} \right] \theta\left(\frac{|\varepsilon|}{2\Delta} - 1 \right) \tag{5}$$

for $z \in \mathbb{C}/\{z\colon \mathrm{Im}\,z = 0, |\mathrm{Re}z| \geq 2\Delta\}$. The second term in Eq. (5) arises because $1/|\chi_{\mathsf{SH}}(\omega_n, \boldsymbol{q})|$ is an increasing function of ω_n; see Supplemental Material [56] for details. This relation allows us to immediately interpret the spectral density $\mathrm{sgn}(\varepsilon)\theta(|\varepsilon| - 2\Delta)\rho_{\boldsymbol{q}}(|\varepsilon|)$ in Eq. (5) as $\mathrm{Im}[1/\chi^R_{\mathsf{SH}}(\varepsilon, \boldsymbol{q})]$, whereas the real part is obtained by taking the principal value of the integral. The full expression for $\rho_{\boldsymbol{q}}(\omega)$ is given in Supplemental Material [56], and its diffusive limit at $\Delta\tau \ll 1$ yields

$$\rho_{\boldsymbol{q}}(\omega) = \frac{4\bar{\omega}^2 - (\bar{q}^4 + \bar{\omega}^2)^2}{\bar{q}^2(\bar{\omega} + 2)(\bar{q}^4 + \bar{\omega}^2)} \times \Pi\left(\frac{(\bar{\omega} - 2)^2(\bar{q}^4 + \bar{\omega}^2)}{\bar{q}^4(4 - \bar{q}^4 - \bar{\omega}^2)} \middle| \frac{\bar{\omega} - 2}{\bar{\omega} + 2} \right) + \frac{\bar{q}^2(4 + \bar{q}^4 + \bar{\omega}^2)}{(\bar{\omega} + 2)(\bar{q}^4 + \bar{\omega}^2)} K\left(\frac{\bar{\omega} - 2}{\bar{\omega} + 2} \right). \tag{6}$$

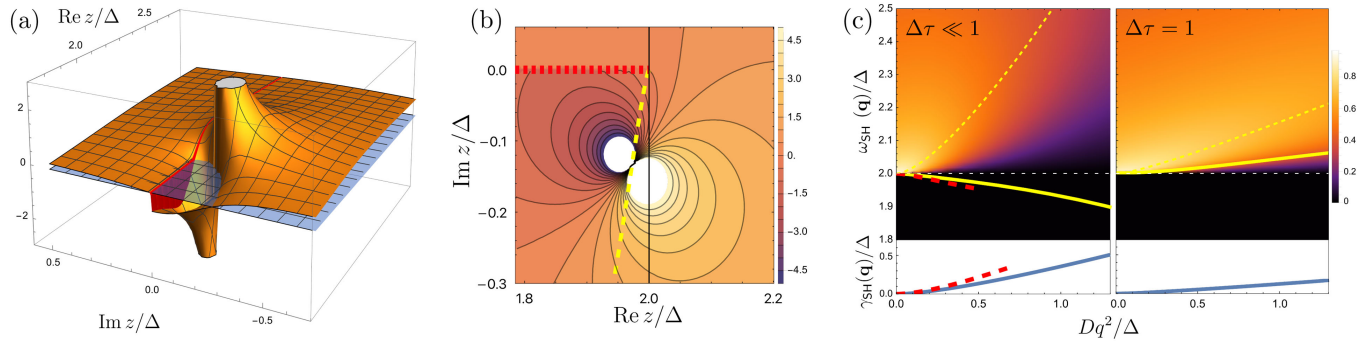

FIG. 2. (a) $\mathrm{Im}\,\chi^{\downarrow}_{\mathrm{SH}}(z,\boldsymbol{q})$ (orange surface) in the complex frequency plane for $Dq^2/\Delta = 0.5$ and $\Delta\tau \ll 1$. The red solid line corresponds to the real axis $\mathrm{Im}\,z = 0$, and the red vertical region indicates the discontinuity in $\mathrm{Im}\,\chi^{\downarrow}_{\mathrm{SH}}(z,\boldsymbol{q})$ along its branch cut. The transparent blue plane marks zero on the vertical axis. (b) Contour plot of $\mathrm{Im}\,\chi^{\downarrow}_{\mathrm{SH}}(z,\boldsymbol{q})$ for the same parameters. The red dashed line indicates the branch cut of $\chi^{\downarrow}_{\mathrm{SH}}(z,\boldsymbol{q})$. The yellow dashed line shows the trajectory of the pole while momentum is varied. (c) Frequency of the SH mode as a function of $\xi^2q^2 \equiv Dq^2/\Delta$ for $\Delta\tau \ll 1$ (left panel) and $\Delta\tau = 1$ (right panel) in 2D, shown with a yellow solid curve. The small-q asymptotic behavior, Eq. (B2), is shown with the dashed red curve. The normalized spectral function $2\arctan(\mathrm{Im}\,\chi^{R}_{\mathrm{SH}}(\omega,\boldsymbol{q}))/\pi \in [0,1]$ is shown with the background color. The yellow dashed line shows the position of the maximum of the spectral function. The horizontal white dashed line denotes the edge of the two-particle continuum. The SH damping rate (blue solid curve) is shown at the bottom.

Here, we define dimensionless variables $\bar{\omega} = \omega/\Delta$ and $\bar{q} = \xi q$, and $\xi = \sqrt{D/\Delta}$ is the coherence length. Also, $\Pi(x|y) = \int_0^{\pi/2} d\alpha/[(1 - x\sin^2\alpha)\sqrt{1 - y^2\sin^2\alpha}]$ is the complete elliptic integral of the 3rd kind, and $K(x) = \Pi(0|x)$. Equation (6) only assumes $|\omega|, v_F q \ll 1/\tau$, but ξq and $|\omega|/\Delta$ can be arbitrary.

The imaginary and real parts of $\chi^{R}_{\mathrm{SH}}(\omega,\boldsymbol{q})$ at $q > 0$ feature a peak at a frequency above 2Δ for arbitrary values of $\Delta\tau$, as shown in Fig. 1. This peak shifts to higher frequencies when momentum is increased. At $q = 0$, the peak is replaced with a square-root singularity at $\omega = 2\Delta$ [1]. Further, assuming the dirty limit, $\xi q \ll 1$ and $0 \le \omega - 2\Delta \ll \Delta$, while keeping the ratio $\Delta\xi^4q^4/(\omega - 2\Delta)$ fixed (i.e., anticipating the $z = 4$ dynamical exponent, defined by the relation $|\omega - 2\Delta| \sim q^z$), we obtain

$$\frac{1}{\chi^{R}_{\mathrm{SH}}} \simeq \frac{\bar{q}^2}{4}\left[\ln\frac{2^6}{\bar{q}^4} - \sum_{s=\pm}(1+su)\ln(u+s) + i\pi(1-u)\right], \quad (7)$$

where $u = \sqrt{1 + 4(\bar{\omega} - 2)/\bar{q}^4} \ge 1$. From Eq. (7), we find that the frequency and width of the peak in χ^{R}_{SH} at $\xi q \ll 1$ [56] scale as

$$\frac{\omega_{\max}(\boldsymbol{q})}{\Delta} \approx 2 + \frac{4\xi^4q^4}{\pi^2}\ln^2\frac{2\sqrt{2}}{\xi q}, \qquad \frac{\gamma_{\max}(\boldsymbol{q})}{\Delta} \sim \xi^4q^4\ln\frac{1}{\xi q}. \quad (8)$$

To calculate the late-time and long-distance behavior of the SH susceptibility, we now proceed to identify its nonanalyticities (e.g., poles) in the complex plane.

SH mode as a pole in the SH susceptibility—The appearance of a peak in $\chi^{R}_{\mathrm{SH}}(\omega,\boldsymbol{q})$ on the real frequency axis is already indicative of a pole in the lower half-plane. However, as emphasized above, the presence of the branch cut implies that $\chi_{\mathrm{SH}}(\omega + i0^+,\boldsymbol{q})$ is not smoothly connected to $\chi_{\mathrm{SH}}(\omega - i0^+,\boldsymbol{q})$. In fact, $\chi_{\mathrm{SH}}(z,\boldsymbol{q})$ does not have any nonanalyticities in the lower half-plane on the physical Riemann sheet. Instead, one has to smoothly continue it through the branch cut into the *unphysical* Riemann sheet and search for a pole there [24,29,31]. The resulting susceptibility, denoted as $\chi^{\downarrow}_{\mathrm{SH}}(z,\boldsymbol{q})$, coincides with Eq. (5) in the upper half-plane, but remains continuous across the interval $\mathrm{Im}\,z = 0, \mathrm{Re}z > 2\Delta$. The structure of $\chi^{\downarrow}_{\mathrm{SH}}(z,\boldsymbol{q})$ is demonstrated in Figs. 2(a) and 2(b), and the explicit formula for it is given in End Matter. Numerical evaluation reveals that $\chi^{\downarrow}_{\mathrm{SH}}(z,\boldsymbol{q})$ indeed has a pole $z_{\boldsymbol{q}}$ in the lower half-plane at any finite momentum q. The SH mode's dispersion is then obtained as $\omega_{\mathrm{SH}}(\boldsymbol{q}) \equiv \mathrm{Re}z_{\boldsymbol{q}}$ and $\gamma_{\mathrm{SH}}(\boldsymbol{q}) \equiv |\,\mathrm{Im}\,z_{\boldsymbol{q}}|$, with both of these quantities exhibiting strong dependence on $\Delta\tau$ [see Fig. 2(c)]. In the dirty limit $\Delta\tau \ll 1$, for $\xi q \ll 1$ we obtain

$$\frac{\omega_{\mathrm{SH}}(\boldsymbol{q})}{\Delta} \approx 2 - \frac{4\xi^4q^4}{\pi^2}\ln^2\frac{2\sqrt{\pi}}{\xi q}, \qquad \frac{\gamma_{\mathrm{SH}}(\boldsymbol{q})}{\Delta} \approx \frac{4\xi^4q^4}{\pi}\ln\frac{2\sqrt{\pi}}{\xi q}. \quad (9)$$

The $z = 4$ scaling of $\omega_{\mathrm{SH}}(\boldsymbol{q})$ with momentum can be also estimated directly from $S_{\boldsymbol{q}}(E)$ in Eq. (4) since the SH mode involves quasiparticles with energy $\omega \gtrsim \Delta$. Expanding $S_{\boldsymbol{q}}(\sqrt{\omega^2 - \Delta^2})$ for such ω, we find that the pole occurs at $|\omega - \Delta| \sim D^2q^4/\Delta$ in the dirty limit. We also emphasize that $\omega_{\mathrm{SH}}(\boldsymbol{q}) < 2\Delta$. In the terminology of Ref. [59], the pole is "hidden" behind the branch cut of $\chi^{\downarrow}_{\mathrm{SH}}(z,\boldsymbol{q})$ on the real axis at $\mathrm{Re}z < 2\Delta$ [see Figs. 2(b) and 2(c)]. Upon increasing

$\Delta\tau$ while keeping ξq fixed, the pole $z_{\boldsymbol{q}}$ shifts to the right. Eventually, its frequency $\omega_{\mathrm{SH}}(\boldsymbol{q})$ exceeds 2Δ—that is, the pole becomes "visible"—and it contributes to the Fourier transform, giving rise to additional exponentially decaying oscillations at frequency $\omega_{\mathrm{SH}}(\boldsymbol{q})$ in $\chi^R_{\mathrm{SH}}(t,\boldsymbol{q})$ [cf. Eq. (10)]. At moderate values of $\Delta\tau \approx 1$, the dispersion develops a quadratic dependence on q [see Fig. 2(c)]. The results of Refs. [29,31] are recovered in the limit $\Delta\tau \to \infty$ (see Supplemental Material [56] for a detailed analysis of the crossover between the dirty and clean regimes). A similar analysis of the SH susceptibility in the complex momentum plane at fixed $\bar{\omega}$ also reveals a pole [56].

Late-time and long-distance SH oscillations—Let us now discuss how the aforementioned pole manifests itself in various asymptotic limits of χ^R_{SH}. First, we consider $\chi^R_{\mathrm{SH}}(t,\boldsymbol{q})$ at late times t and fixed momentum, which describes a response to a sudden, spatially periodic perturbation. For arbitrary $\Delta\tau$, we find

$$\chi^R_{\mathrm{SH}}(t,\boldsymbol{q}) \simeq 2\,\mathrm{Im}[Z_{\boldsymbol{q}} e^{-i\omega_{\mathrm{SH}}(\boldsymbol{q})t}]e^{-\gamma_{\mathrm{SH}}(\boldsymbol{q})t}\theta[\omega_{\mathrm{SH}}(\boldsymbol{q})-2\Delta] - \frac{2\sin(2\Delta t)}{\pi t^2}\partial_\omega\,\mathrm{Im}\,\chi^R_{\mathrm{SH}}(\omega,\boldsymbol{q})_{\omega=2\Delta+0^+}, \quad (10)$$

where $Z_{\boldsymbol{q}}$ is the residue of $\chi^{\downarrow}_{\mathrm{SH}}(z,\boldsymbol{q})$ at $z_{\boldsymbol{q}}$. The asymptotic late-time behavior is determined by the second term stemming from the continuum edge at $\omega = 2\Delta$ in $\mathrm{Im}\,\chi^R_{\mathrm{SH}}$. These oscillations at frequency 2Δ decay as $1/t^2$, in contrast to the conventional $\sim 1/\sqrt{t}$ decay at $q = 0$ [1]. The first term in Eq. (10) originates from the pole $z_{\boldsymbol{q}}$, provided that its real part, $\omega_{\mathrm{SH}}(\boldsymbol{q})$, exceeds 2Δ. Although this exponentially decaying contribution is subleading, interestingly, its frequency is q-dependent. In the dirty limit, the pole is "hidden" by the branch cut [$\omega_{\mathrm{SH}}(\boldsymbol{q}) < 2\Delta$, see Figs. 2(a) and 2(b)], so its contribution to χ^R_{SH} is strongly incoherent and does not produce oscillations. Thus for $\Delta\tau \ll 1$ and $\xi q \ll 1$, Eq. (10) yields

$$\chi^R_{\mathrm{SH}}(t,\boldsymbol{q}) \approx -\sin(2\Delta t)/[\Delta t^2(\xi q)^6 \ln^2(\xi q/2)]. \quad (11)$$

At moderate disorder (or large momentum), the SH pole shifts into the right half-plane ($\omega_{\mathrm{SH}} > 2\Delta$) and becomes "visible" [cf. Fig. 2(c)], resulting in a coherent feature in χ^R_{SH} and additional oscillations [first term in Eq. (10)]. The "critical" q_c at which these oscillations first appear [i.e., $\omega_{\mathrm{SH}}(q_c) = 2\Delta$] is analyzed in Supplemental Material [56].

The long-distance oscillations of $\chi^R_{\mathrm{SH}}(\omega,\boldsymbol{r})$ at a fixed frequency ω are closely related to the pole in $\chi^{\downarrow}_{\mathrm{SH}}$ in the complex momentum space. These oscillations correspond to a spatially-local periodic external drive and exist for $\omega > 2\Delta$ only. In 2D and in the dirty limit, $\Delta\tau \ll 1$, we find

$$\mathrm{Im}\,\chi^R_{\mathrm{SH}}(\omega,\boldsymbol{r}) \simeq \frac{2^{1/4}\sqrt{\xi_\omega/r}}{\sqrt{\pi}\xi^2 \ln\frac{2^4\Delta}{\omega-2\Delta}} e^{-r/\xi_\omega} \sin\left(\frac{r}{\xi_\omega}+\frac{\pi}{8}\right), \quad (12)$$

where $\xi_\omega = \xi\{|\ln\{[(\omega/\Delta)-2]/2^4\}|^2/\{\pi^2[(\omega/\Delta)-2]\}\}^{1/4}$ is the period of oscillations diverging at the threshold $\omega = 2\Delta$.

The long-distance and late-time behavior of $\chi_{\mathrm{SH}}(t,\boldsymbol{r})$ in the regime $\Delta\tau \ll 1$ is subdiffusive, featuring oscillations as a function of $\varkappa = \pi^2(r/\xi)^4/(\Delta t)\ln^2(\Delta t)$ with an approximate dynamical exponent $z = 4$ (which implies the relation $r \sim t^{1/z}$). In 2D, for $\varkappa \gg 1$, we find

$$\chi^R_{\mathrm{SH}}(t,\boldsymbol{r}) \simeq \frac{2^{3/4} e^{-\frac{3\sqrt{3}}{8}\varkappa^{1/3}}}{\sqrt{3}\pi\xi^2 t \ln(\Delta t)} \cos\left(\frac{3}{8}\varkappa^{1/3} - 2\Delta t\right). \quad (13)$$

In the opposite regime, $\Delta\tau \gg 1$, the amplitude SH fluctuations propagate diffusively, with $z = 2$. Oscillations [Eq. (13)] can be induced by a quenched perturbation affecting a local gap magnitude. The results in 3D are qualitatively similar to Eqs. (12) and (13) and are presented in Supplemental Material [56]. The analytic results [Eqs. (12) and (13)] are benchmarked against direct numerical evaluation of χ^R_{SH} shown in Fig. 3.

SH mode and the nonlinear current response—The results for χ_{SH} outlined above can be directly probed via the electromagnetic response to an external harmonic

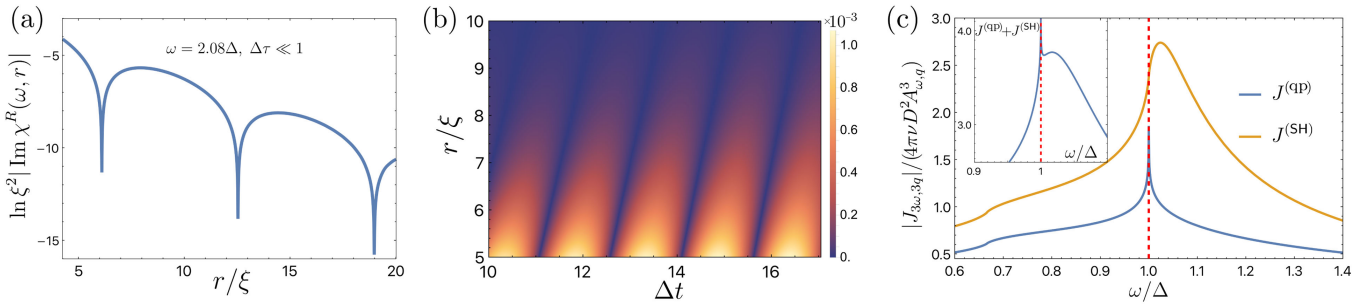

FIG. 3. Oscillations in (a) $\ln\xi^2|\,\mathrm{Im}\,\chi^R_{\mathrm{SH}}(\omega,r)|$ and in (b) $|\xi^2\chi^R_{\mathrm{SH}}(t,r)/\Delta|$ in 2D, and in the dirty limit $\Delta\tau \ll 1$. (c) The absolute value of the individual contributions to the current for $Dq^2/\Delta = 1/8$ for $\Delta\tau \ll 1$. The red dashed line indicates the $q = 0$ resonance at $\omega = \Delta$. The blue (orange) curve corresponds to the quasiparticle (Schmid-Higgs) contribution. The inset shows the total current. Additional details on the dependence of the current on Dq^2/Δ are provided in Supplemental Material [56].

vector potential $\boldsymbol{A}(t,\boldsymbol{r}) = \boldsymbol{A}_{\omega,\boldsymbol{q}} e^{i\boldsymbol{q}\cdot\boldsymbol{r}-i\omega t}$. As is well known, at cubic order in $\boldsymbol{A}_{\omega,\boldsymbol{q}}$, induced corrections to the amplitude fluctuations at frequency 2ω and momentum $2\boldsymbol{q}$ lead to the current oscillations at frequency 3ω and momentum $3\boldsymbol{q}$—the effect known as third harmonic generation (THG) [8,19,20,25,26]. After evaluating the diagrams familiar from the $q = 0$ case [26], we find that the resulting paramagnetic contribution to the current (which is absent in the clean case [6,20]) consists of two terms, $\boldsymbol{J}_{3\omega,3\boldsymbol{q}} = \boldsymbol{J}^{(\mathrm{qp})}_{3\omega,3\boldsymbol{q}} + \boldsymbol{J}^{(\mathrm{SH})}_{3\omega,3\boldsymbol{q}}$ (see End Matter). The first term corresponds to a direct quasiparticle (qp) channel, and the second one involves the SH susceptibility:

$$\boldsymbol{J}^{(\mathrm{SH})}_{3\omega,3\boldsymbol{q}} = 4\pi\nu D^2 \chi^R_{\mathrm{SH}}(2\omega,2q)\mathcal{B}^R_{\mathrm{SH}}(\omega,q)|\boldsymbol{A}_{\omega,\boldsymbol{q}}|^2\boldsymbol{A}_{\omega,\boldsymbol{q}}. \tag{14}$$

The lengthy expression for $\mathcal{B}^R_{\mathrm{SH}}(\omega,q)$ is given in Supplemental Material [56]. Unlike the SH susceptibility $\chi^R_{\mathrm{SH}}(2\omega,2q)$, $\mathcal{B}^R_{\mathrm{SH}}(\omega,q)$ does not exhibit any sharp nonanalytic features in the limit $q \to 0$ and $\omega \to \Delta$, and it could be replaced in Eq. (14) with its limiting value $\mathcal{B}^R_{\mathrm{SH}}(\Delta,0) \approx -1.55 - 1.27i$. Consequently, for $|\omega - \Delta| \ll \Delta$, the current $\boldsymbol{J}^{(\mathrm{SH})}_{3\omega,3\boldsymbol{q}}$ is essentially governed by the SH susceptibility and exhibits a peak at a frequency $\omega_{\max}(\boldsymbol{q})/2 > \Delta$ with the height that scales as $1/(\xi q)^2$; see Eq. (8) and Fig. 3(c). In contrast, we find that the peak in the "quasiparticle" contribution $\boldsymbol{J}^{(\mathrm{qp})}_{3\omega,3\boldsymbol{q}}$ remains fixed at Δ even for $q \neq 0$, as shown in Fig. 2(c). Intuitively, this is expected because the momentum-resolved collective dynamics of the order parameter fluctuations is very distinct from individual quasiparticle excitations. Since $\boldsymbol{J}^{(\mathrm{qp})}_{3\omega,3\boldsymbol{q}}$ at $\omega = \omega_{\max}(\boldsymbol{q})/2$ grows as $\ln[1/(\xi q)]$ only (see End Matter), the peak in the SH contribution dominates the quasiparticle contribution at $\xi q \ll 1$. The pair-breaking effects (e.g., magnetic impurities) will broaden both peaks, thereby establishing a lower bound on q for observation of the SH peak in the THG. Thus, the emergence of an additional peak at a frequency above Δ in the finite-momentum current provides an unambiguous signature of the amplitude SH fluctuations and allows for a direct investigation of their dynamics summarized by Eqs. (11)–(13).

Conclusions—In this Letter, we studied the spatially-resolved dynamics of the order parameter amplitude (SH) fluctuations in BCS superconductors with nonmagnetic impurities. We identified a pole on the unphysical Riemann sheet of the SH susceptibility, associated with the oscillatory mode exhibiting subdiffusive $z = 4$ spreading in the dirty limit. This pole also produces a peak in the spectral function above the edge of the two-particle continuum, even though the frequency of the SH mode itself can be below 2Δ for sufficiently strong disorder. We also calculated the contribution of the SH mode to the nonlinear current response, focusing on the THG. We found that at finite wave vectors, the THG current exhibits an additional peak in its amplitude, shifted away from the conventional resonance at $\omega = \Delta$. This extra peak arises solely from the dynamics of the amplitude SH mode. Importantly, both disorder and finite wave vectors are essential for this effect. Without disorder, the SH mode would not contribute to the current [20], and at zero wave vector, multiple processes conflate into a single peak at Δ [26], making it difficult to disentangle the SH contribution. Our findings could be directly tested with spatially-resolved terahertz and Raman spectroscopic probes [7–10]. Moreover, a finite wave vector can be imprinted in the current response in thin films with high-frequency surface acoustic waves [60,61], diffraction gratings and micropatterning [62], finite spot size of the pump pulse [6,63], or adding extra layers of a 2D van der Waals material with a Moiré superlattice. Another promising possibility is to use spatially-inhomogeneous Feshbach modulation of the interaction strength in disordered cold gases [64] to directly quench the local value of the gap and study its spatial relaxation [65].

Acknowledgments—We thank A. Chubukov, A. Mel'nikov, V. Kravtsov, S. Raghu, and A. Levchenko for fruitful discussions. The work of P. A. N. was supported in part by the U.S. Department of Energy, Office of Basic Energy Sciences, Division of Materials Sciences and Engineering, under Contract No. DE-AC02-76SF00515. The work of I. S. B. was supported by the Russian Ministry of Science and Higher Education and by the Basic Research Program of HSE. I. S. B. acknowledges personal support from the Foundation for the Advancement of Theoretical Physics and Mathematics "BASIS."

[1] V. Vaks, V. Galitskii, and A. Larkin, Collective excitations in a superconductor, Sov. Phys. JETP **14**, 1177 (1962).
[2] A. Schmid, The approach to equilibrium in a pure superconductor: The relaxation of the Cooper pair density, Phys. Status Solidi (b) **8**, 129 (1968).
[3] S. N. Artemenko and A. F. Volkov, Electric fields and collective oscillations in superconductors, Sov. Phys. Usp. **22**, 295 (1979).
[4] I. O. Kulik, O. Entin-Wohlman, and R. Orbach, Pair susceptibility and mode propagation in superconductors: A microscopic approach, J. Low Temp. Phys. **43**, 591 (1981).
[5] P. I. Arseev, S. O. Loiko, and N. K. Fedorov, Theory of gauge-invariant response of superconductors to an external electromagnetic field, Phys. Usp. **49**, 1 (2006).
[6] R. Shimano and N. Tsuji, Higgs mode in superconductors, Annu. Rev. Condens. Matter Phys. **11**, 103 (2020).
[7] R. Matsunaga, Y. I. Hamada, K. Makise, Y. Uzawa, H. Terai, Z. Wang, and R. Shimano, Higgs amplitude mode in the BCS superconductors $Nb_{1-x}Ti_xN$ induced by terahertz pulse excitation, Phys. Rev. Lett. **111**, 057002 (2013).
[8] R. Matsunaga, N. Tsuji, H. Fujita, A. Sugioka, K. Makise, Y. Uzawa, H. Terai, Z. Wang, H. Aoki, and R. Shimano,

Light-induced collective pseudospin precession resonating with Higgs mode in a superconductor, Science **345**, 1145 (2014).

[9] D. Sherman, U. S. Pracht, B. Gorshunov, S. Poran, J. Jesudasan, M. Chand, P. Raychaudhuri, M. Swanson, N. Trivedi, A. Auerbach *et al.*, The Higgs mode in disordered superconductors close to a quantum phase transition, Nat. Phys. **11**, 188 (2015).

[10] R. Grasset, T. Cea, Y. Gallais, M. Cazayous, A. Sacuto, L. Cario, L. Benfatto, and M.-A. Méasson, Higgs-mode radiance and charge-density-wave order in 2H-$NbSe_2$, Phys. Rev. B **97**, 094502 (2018).

[11] K. Katsumi, J. Fiore, M. Udina, R. Romero, D. Barbalas, J. Jesudasan, P. Raychaudhuri, G. Seibold, L. Benfatto, and N. P. Armitage, Revealing novel aspects of light-matter coupling by terahertz two-dimensional coherent spectroscopy: The case of the amplitude mode in superconductors, Phys. Rev. Lett. **132**, 256903 (2024).

[12] i. c. v. Kos, A. J. Millis, and A. I. Larkin, Gaussian fluctuation corrections to the BCS mean-field gap amplitude at zero temperature, Phys. Rev. B **70**, 214531 (2004).

[13] R. Combescot, M. Y. Kagan, and S. Stringari, Collective mode of homogeneous superfluid Fermi gases in the BEC-BCS crossover, Phys. Rev. A **74**, 042717 (2006).

[14] R. A. Barankov and L. S. Levitov, Synchronization in the BCS pairing dynamics as a critical phenomenon, Phys. Rev. Lett. **96**, 230403 (2006).

[15] E. A. Yuzbashyan, O. Tsyplyatyev, and B. L. Altshuler, Relaxation and persistent oscillations of the order parameter in fermionic condensates, Phys. Rev. Lett. **96**, 097005 (2006).

[16] M. Dzero, E. A. Yuzbashyan, and B. L. Altshuler, Cooper pair turbulence in atomic Fermi gases, Europhys. Lett. **85**, 20004 (2009).

[17] D. Podolsky, A. Auerbach, and D. P. Arovas, Visibility of the amplitude (Higgs) mode in condensed matter, Phys. Rev. B **84**, 174522 (2011).

[18] S. Gazit, D. Podolsky, and A. Auerbach, Fate of the Higgs mode near quantum criticality, Phys. Rev. Lett. **110**, 140401 (2013).

[19] N. Tsuji and H. Aoki, Theory of Anderson pseudospin resonance with Higgs mode in superconductors, Phys. Rev. B **92**, 064508 (2015).

[20] T. Cea, C. Castellani, and L. Benfatto, Nonlinear optical effects and third-harmonic generation in superconductors: Cooper pairs versus Higgs mode contribution, Phys. Rev. B **93**, 180507(R) (2016).

[21] A. Moor, A. F. Volkov, and K. B. Efetov, Amplitude Higgs mode and admittance in superconductors with a moving condensate, Phys. Rev. Lett. **118**, 047001 (2017).

[22] S. Fischer, M. Hecker, M. Hoyer, and J. Schmalian, Short-distance breakdown of the Higgs mechanism and the robustness of the BCS theory for charged superconductors, Phys. Rev. B **97**, 054510 (2018).

[23] P. Shen and M. Dzero, Gaussian fluctuation corrections to a mean-field theory of complex hidden order in URu_2Si_2, Phys. Rev. B **98**, 125131 (2018).

[24] H. Kurkjian, S. N. Klimin, J. Tempere, and Y. Castin, Pair-breaking collective branch in BCS superconductors and superfluid Fermi gases, Phys. Rev. Lett. **122**, 093403 (2019).

[25] Y. Murotani and R. Shimano, Nonlinear optical response of collective modes in multiband superconductors assisted by nonmagnetic impurities, Phys. Rev. B **99**, 224510 (2019).

[26] M. Silaev, Nonlinear electromagnetic response and Higgs-mode excitation in BCS superconductors with impurities, Phys. Rev. B **99**, 224511 (2019).

[27] Z. Sun, M. M. Fogler, D. N. Basov, and A. J. Millis, Collective modes and terahertz near-field response of superconductors, Phys. Rev. Res. **2**, 023413 (2020).

[28] P. A. Lee and J. F. Steiner, Detection of collective modes in unconventional superconductors using tunneling spectroscopy, Phys. Rev. B **108**, 174503 (2023).

[29] D. Phan and A. V. Chubukov, Following the Higgs mode across the BCS-BEC crossover in two dimensions, Phys. Rev. B **107**, 134519 (2023).

[30] Y. Du, G. Liu, W. Ruan, Z. Fang, K. Watanabe, T. Taniguchi, R. Liu, J.-X. Li, and X. Xi, Unveiling resilient superconducting fluctuations in atomically thin $nbse_2$ through Higgs mode spectroscopy, Phys. Rev. Lett. **134**, 066002 (2025).

[31] V. A. Andrianov and V. N. Popov, Hydrodynamic action and Bose spectrum of superfluid Fermi systems, Theor. Math. Phys. **28**, 829 (1976).

[32] R. V. Carlson and A. M. Goldman, Superconducting order-parameter fluctuations below T_c, Phys. Rev. Lett. **31**, 880 (1973).

[33] R. A. Smith, M. Y. Reizer, and J. W. Wilkins, Suppression of the order parameter in homogeneous disordered superconductors, Phys. Rev. B **51**, 6470 (1995).

[34] M. Reizer, Electron-electron relaxation in two-dimensional impure superconductors, Phys. Rev. B **61**, 7108 (2000).

[35] M. Mondal, A. Kamlapure, M. Chand, G. Saraswat, S. Kumar, J. Jesudasan, L. Benfatto, V. Tripathi, and P. Raychaudhuri, Phase fluctuations in a strongly disordered s-wave NbN superconductor close to the metal-insulator transition, Phys. Rev. Lett. **106**, 047001 (2011).

[36] T. Cea, D. Bucheli, G. Seibold, L. Benfatto, J. Lorenzana, and C. Castellani, Optical excitation of phase modes in strongly disordered superconductors, Phys. Rev. B **89**, 174506 (2014).

[37] T. Cea, C. Castellani, G. Seibold, and L. Benfatto, Nonrelativistic dynamics of the amplitude (Higgs) mode in superconductors, Phys. Rev. Lett. **115**, 157002 (2015).

[38] A. V. Shtyk and M. V. Feigel'man, Collective modes and ultrasonic attenuation in a pseudogapped superconductor, Phys. Rev. B **96**, 064523 (2017).

[39] A. Kamenev, *Field Theory of Non-Equilibrium Systems* (Cambridge University Press, Cambridge, England, 2023).

[40] Y. Li and M. Dzero, Amplitude Higgs mode in superconductors with magnetic impurities, Phys. Rev. B **109**, 054520 (2024).

[41] Y. Li and M. Dzero, Collective modes in terahertz field response of superconductors with paramagnetic impurities, arXiv:2403.03980.

[42] B. Fan and A. M. G. García, Quenched dynamics and pattern formation in clean and disordered Bogoliubov-de Gennes superconductors, SciPost Phys. **17**, 049 (2024).

[43] K. Wang, R. Boyack, and K. Levin, The Higgs-amplitude mode in the optical conductivity in the presence of a supercurrent: Gauge invariant forumulation, Phys. Rev. B **111**, 144512 (2025).
[44] P. W. Anderson, Theory of dirty superconductors, J. Phys. Chem. Solids **11**, 26 (1959).
[45] A. A. Abrikosov and L. P. Gor'kov, On the theory of superconducting alloys, I. The electrodynamics of alloys at absolute zero, Sov. Phys. JETP **8**, 1090 (1959).
[46] A. A. Abrikosov and L. P. Gor'kov, Superconducting alloys at finite temperatures, Sov. Phys. JETP **9**, 220 (1959).
[47] S. Maekawa and H. Fukuyama, Localization effects in two-dimensional superconductors, J. Phys. Soc. Jpn. **51**, 1380 (1982).
[48] S. Maekawa, H. Ebisawa, and H. Fukuyama, Theory of dirty superconductors in weakly localized regime, J. Phys. Soc. Jpn. **53**, 2681 (1984).
[49] A. M. Finkel'stein, Superconducting transition temperature in amorphous films, JETP Lett. **45**, 46 (1987).
[50] A. M. Finkel'stein, Suppression of superconductivity in homogeneously disordered systems, Physica (Amsterdam) **197B**, 636 (1994).
[51] A. Larkin and Y. N. Ovchinnikov, Density of states in inhomogeneous superconductors, Sov. Phys. JETP **34**, 1144 (1972).
[52] J. S. Meyer and B. D. Simons, Gap fluctuations in inhomogeneous superconductors, Phys. Rev. B **64**, 134516 (2001).
[53] M. V. Feigel'man and M. A. Skvortsov, Universal broadening of the Bardeen-Cooper-Schrieffer coherence peak of disordered superconducting films, Phys. Rev. Lett. **109**, 147002 (2012).
[54] The coupling between the amplitude and phase fluctuations of the order parameter $\Delta = |\Delta| e^{i\theta}$ vanishes after averaging over disorder in the BCS limit due to the effective particle-hole symmetry [33,55].
[55] E. Andriyakhina, P. Nosov, S. Raghu, and I. Burmistrov, Quantum fluctuations and multifractally enhanced superconductivity in disordeed thin films, J. Low Temp. Phys. **217**, 187 (2024).
[56] See Supplemental Material at http://link.aps.org/supplemental/10.1103/x12p-q7bj for additional technical details and derivations of the main equations, which includes additional Refs. [57,58].
[57] P. A. Lee and T. V. Ramakrishnan, Disordered electronic systems, Rev. Mod. Phys. **57**, 287 (1985).
[58] A. D. Mirlin, Statistics of energy levels and eigenfunctions in disordered systems, Phys. Rep. **326**, 259 (2000).
[59] A. Klein, D. L. Maslov, and A. V. Chubukov, Hidden and mirage collective modes in two dimensional Fermi liquids, npj Quantum Mater. **5**, 55 (2020).
[60] R. L. Willett, R. R. Ruel, M. A. Paalanen, K. W. West, and L. N. Pfeiffer, Enhanced finite-wave-vector conductivity at multiple even-denominator filling factors in two-dimensional electron systems, Phys. Rev. B **47**, 7344 (1993).
[61] R. L. Willett, R. R. Ruel, K. W. West, and L. N. Pfeiffer, Experimental demonstration of a Fermi surface at one-half filling of the lowest Landau level, Phys. Rev. Lett. **71**, 3846 (1993).
[62] P. H. McGuinness, E. Zhakina, M. König, M. D. Bachmann, C. Putzke, P. J. W. Moll, S. Khim, and A. P. Mackenzie, Low-symmetry nonlocal transport in microstructured squares of delafossite metals, Proc. Natl. Acad. Sci. U.S.A. **118**, e2113185118 (2021).
[63] P. Dyke, S. Musolino, H. Kurkjian, D. J. M. Ahmed-Braun, A. Pennings, I. Herrera, S. Hoinka, S. J. J. M. F. Kokkelmans, V. E. Colussi, and C. J. Vale, Higgs oscillations in a unitary Fermi superfluid, Phys. Rev. Lett. **132**, 223402 (2024).
[64] I. Carusotto and Y. Castin, Atom interferometric detection of the pairing order parameter in a Fermi gas, Phys. Rev. Lett. **94**, 223202 (2005).
[65] M. Endres, T. Fukuhara, D. Pekker, M. Cheneau, P. Schauß, C. Gross, E. Demler, S. Kuhr, and I. Bloch, The 'Higgs' amplitude mode at the two-dimensional superfluid/Mott insulator transition, Nature (London) **487**, 454 (2012).

End Matter

Appendix A: Formula for $\chi^{\downarrow}_{\mathrm{SH}}(z,\boldsymbol{q})$—The explicit formula for the function $\chi^{\downarrow}_{\mathrm{SH}}(z,\boldsymbol{q})$ is given by

$$\frac{1}{\chi^{\downarrow}_{\mathrm{SH}}(z,\boldsymbol{q})} = \begin{cases} [\chi_{\mathrm{SH}}(z,\boldsymbol{q})]^{-1}, & \mathrm{Im}\, z > 0 \\ [\chi_{\mathrm{SH}}(z,\boldsymbol{q})]^{-1} + 2i\rho_{\boldsymbol{q}}(z), & \mathrm{Im}\, z \le 0. \end{cases} \tag{A1}$$

Here $[\chi_{\mathrm{SH}}(z,\boldsymbol{q})]^{-1}$ is defined in Eq. (5), and $\rho_{\boldsymbol{q}}(z)$ is the analytic continuation of $\rho_{\boldsymbol{q}}(\omega)$, given in Eq. (6) for $\Delta\tau \ll 1$ and for arbitrary $\Delta\tau$ in Supplemental Material [56], from $\omega \ge 2\Delta$ into the lower complex half-plane.

Appendix B: SH pole for $\Delta\tau \ll 1$—Next, we analytically derive the expression for the pole in the dirty limit. Instead of using our global integral representation in Eq. (A1), we follow an equivalent route by analytically continuing the approximate expression for $\chi^{R}_{\mathrm{SH}}(\omega,\boldsymbol{q})$ [given in Eq. (7) on the real axis at $\omega > 2\Delta$] into the lower half plane, thereby ensuring the smoothness of the resulting function across the cut. After setting the inverse of the rhs of Eq. (7) to zero and treating u as a complex variable, we obtain the following equation: $\ln(u^*\bar{q}^2/8) = i\pi(1-u^*)/2$. Its solution is given by $u^* \simeq 2 + 2i[1 - W(4\pi/\bar{q}^2)]/\pi$, where $W(y)$ is the Lambert function defined as a solution of the equation $W \exp W = y$. For $y \gg 1$, we find $W(y) \simeq \ln(y/\ln y)$, and thus we can assume that $W(4\pi/\bar{q}^2) \gg 1$. The resulting behavior near the pole is given by

$$\chi^{\downarrow}_{\mathrm{SH}}(z,\boldsymbol{q}) \simeq \frac{Z_{\boldsymbol{q}}}{z - z_{\boldsymbol{q}}}, \qquad \frac{Z_{\boldsymbol{q}}}{\Delta} \simeq \frac{4\bar{q}^2}{\pi^2}\left[W\left(\frac{4\pi}{\bar{q}^2}\right) + i\pi\right], \tag{B1}$$

and the position of the pole $z_{\boldsymbol{q}}$ is given by

$$\frac{z_{\boldsymbol{q}}}{\Delta} \simeq 2 - \frac{\bar{q}^4}{\pi^2}[W(4\pi/\bar{q}^2) - 1]^2 - \frac{2i\bar{q}^4}{\pi}[W(4\pi/\bar{q}^2) - 1]. \quad \text{(B2)}$$

Within the leading logarithmic accuracy, we obtain Eq. (9).

The position of the pole in the complex momentum plane can also be found from Eq. (7). After rewriting the expression in Eq. (7) as

$$\chi^R_{\mathrm{SH}}(\omega, \boldsymbol{q}) \simeq 2\sqrt{\frac{u^2-1}{\bar{\omega}-2}}\left[\ln\frac{2^4}{\bar{\omega}-2} + u\ln\frac{u-1}{u+1} + i\pi(1-u)\right]^{-1} \quad \text{(B3)}$$

for $\omega > 2\Delta$ and $\Delta\tau \ll 1$, setting the inverse of this expression to zero, finding the solution $\tilde{u}_*$, and converting it back to momentum $\bar{q}$, we obtain

$$\chi^R_{\mathrm{SH}}(\omega, \boldsymbol{q}) \simeq \frac{\tilde{Z}_\omega}{\bar{q}^2 - \bar{q}^2_\omega}, \qquad \bar{q}^2_\omega \simeq \frac{2\pi\sqrt{\bar{\omega}-2}}{\ln\frac{2^4}{\bar{\omega}-2}}\left[i + \frac{\pi}{\ln\frac{2^4}{\bar{\omega}-2}}\right], \quad \text{(B4)}$$

and $\tilde{Z}_\omega \simeq 1/|\ln[(\bar{\omega}-2)^{1/4}/2]|$ is the residue at $\bar{q}^2_\omega$. Its Fourier transform leads to Eqs. (12) and (13) [56].

Appendix C: Explicit expressions for the nonlinear current response—The nonlinear current response at $q = 0$ was analyzed in [26]. Here, we extend that analysis to finite q. The diagrams determining the paramagnetic contribution to the current are identical to those in [26]. A straightforward calculation yields Eq. (14), where the function $\mathcal{B}^R_{\mathrm{SH}}(\omega, q)$ is expressed as a product of two fermionic loops, each connecting two external vector potential vertices to the SH susceptibility:

$$\mathcal{B}^R_{\mathrm{SH}}(\omega, q) = -2\pi B^R_1(\omega, 2q) B^R_2(\omega, 2q). \quad \text{(C1)}$$

The expressions for $B_1(\omega_n, q)$ and $B_2(\omega_n, q)$ on the Matsubara axis are given in Supplemental Material [56]. Here, we only provide the result after analytic continuation for $\Delta\tau \ll 1$ and at $T = 0$:

$$\frac{B^R_1(\omega, q)}{\Delta} = \int_0^\omega \frac{d\varepsilon}{2\pi i} F^{RA}_{\omega,q}(\varepsilon) + \int_{-\infty}^{+\infty} \frac{d\varepsilon}{4\pi i}\mathrm{sgn}(\varepsilon - \omega) F^{RR}_{\omega,q}(\varepsilon),$$

$$F^{Rs}_{\omega,q}(\varepsilon) = \frac{\Delta^2 + 3\varepsilon^2 - \omega^2 - E^R_{\varepsilon+\omega}E^s_{\varepsilon-\omega}}{(Dq^2 + E^R_{\varepsilon+\omega} + E^s_{\varepsilon-\omega})E^R_\varepsilon E^R_{\varepsilon+\omega}E^s_{\varepsilon-\omega}},$$

$$E^R_\varepsilon = \theta(\Delta - |\varepsilon|)\sqrt{\Delta^2 - \varepsilon^2} - i\theta(|\varepsilon| - \Delta)\mathrm{sgn}(\varepsilon)\sqrt{\varepsilon^2 - \Delta^2} \quad \text{(C2)}$$

and $E^A_\varepsilon = E^R_{-\varepsilon}$. Similarly, for B^R_2, we find

$$\frac{B^R_2(\omega, q)}{\Delta} = \int_0^\omega \frac{d\varepsilon}{2\pi i}\Phi^{RAA}_{\omega,q}(\varepsilon) + \int_\omega^{2\omega} \frac{d\varepsilon}{2\pi i}\Phi^{RRA}_{\omega,q}(\varepsilon) + \int_{-\infty}^{+\infty} \frac{d\varepsilon}{4\pi i}\mathrm{sgn}(\varepsilon - 2\omega)\Phi^{RRR}_{\omega,q}(\varepsilon), \quad \text{(C3)}$$

where we also define

$$\Phi^{Rs\sigma}_{\omega,q}(\varepsilon) = \frac{1}{(Dq^2 + E^R_{\varepsilon+\omega} + E^s_{\varepsilon-\omega})E^R_{\varepsilon+\omega}E^s_{\varepsilon-\omega}} \times \left\{\left(\frac{1}{E^R_{\varepsilon+2\omega}} + \frac{1}{E^\sigma_{\varepsilon-2\omega}}\right) \times \left(\Delta^2 + \varepsilon^2 - \omega^2 - E^R_{\varepsilon+\omega}E^s_{\varepsilon-\omega}\right) + 2\varepsilon\left(\frac{\varepsilon+2\omega}{E^R_{\varepsilon+2\omega}} + \frac{\varepsilon-2\omega}{E^\sigma_{\varepsilon-2\omega}}\right)\right\}. \quad \text{(C4)}$$

Finally, the quasiparticle contribution, $J^{(\mathrm{qp})}_{3\omega,3q}$, is given by

$$J^{(\mathrm{qp})}_{3\omega,3q} = -4\pi\nu D^2 B^R_3(\omega, 2q)|\boldsymbol{A}_{\omega,\boldsymbol{q}}|^2\boldsymbol{A}_{\omega,\boldsymbol{q}}, \quad \text{(C5)}$$

where $B_3(\omega_n, q)$ on the Matsubara axis is provided in Supplemental Material [56]. The real frequency expression for $B^R_3(\omega, q)$ is the same as for $B^R_2(\omega, q)$ in Eq. (C3), but with $\Phi^{Rs\sigma}_{\omega,q}(\varepsilon)$ replaced by $W^{Rs\sigma}_{\omega,q}(\varepsilon)$, where

$$W^{Rs\sigma}_{\omega,q}(\varepsilon) = \frac{1}{(Dq^2 + E^R_{\varepsilon+\omega} + E^s_{\varepsilon-\omega})E^R_\varepsilon}\left\{\left(\frac{\Delta}{E^R_{\varepsilon+2\omega}} + \frac{\Delta}{E^\sigma_{\varepsilon-2\omega}}\right) \times \left(1 + \frac{\omega^2 - \Delta^2 - 3\varepsilon^2}{E^R_{\varepsilon+\omega}E^s_{\varepsilon-\omega}}\right) - \frac{\varepsilon}{\Delta}\left(1 + \frac{3\Delta^2 - \omega^2 + \varepsilon^2}{E^R_{\varepsilon+\omega}E^s_{\varepsilon-\omega}}\right) \times \left(\frac{\varepsilon+2\omega}{E^R_{\varepsilon+2\omega}} + \frac{\varepsilon-2\omega}{E^\sigma_{\varepsilon-2\omega}}\right)\right\}. \quad \text{(C6)}$$

Near the resonance at $\omega \approx \Delta$, we find a logarithmic divergence

$$B^R_3(\omega, q) \approx \frac{1}{\pi}\frac{1}{Dq^2/\Delta + 1 - i\sqrt{3}}\ln\frac{\Delta}{|\omega - \Delta|}. \quad \text{(C7)}$$

Therefore, $J^{(\mathrm{qp})}_{3\omega_{\max}(q)/2,3q}$ increases as $\ln 1/(\xi q)$ for $\xi q \ll 1$. The expressions for arbitrary $\Delta\tau$ can be obtained by replacing factors $(Dq^2 + E^R_{\varepsilon+\omega} + E^s_{\varepsilon-\omega})^{-1}$ in Eqs. (C2), (C4), and (C6) with $S_{\boldsymbol{q}}(E^R_{\varepsilon+\omega} + E^s_{\varepsilon-\omega})$.